ACS APPLIED MATERIALS & INTERFACES

Research Article

www.acsami.org

Probing Thermally Induced Decomposition of Delithiated $Li_{1.2-x}Ni_{0.15}Mn_{0.55}Co_{0.1}O_2$ by in Situ High-Energy X-ray Diffraction

Chi-kai Lin,[†] Ying Piao,[†,§] Yongchun Kan,[†,⊥] Javier Bareño,[†] Ira Bloom,[†] Yang Ren,[‡] Khalil Amine,[†] and Zonghai Chen*,[†]

[†]Chemical Sciences and Engineering Division and [‡]X-ray Science Division, Advanced Photon Source, Argonne National Laboratory, 9700 South Cass Avenue, Argonne, Illinois 60439, United States

[§]Key Laboratory of Physics and Technology for Advanced Batteries (Ministry of Education), College of Physics, Jilin University, Changchun, 130012, P. R. China

[⊥]State Key Laboratory of Fire Science, University of Science and Technology of China, Hefei, Anhui 230026, P. R. China

ABSTRACT: Safety of lithium-ion batteries has been a major barrier to large-scale applications. For better understanding the failure mechanism of battery materials under thermal abuse, the decomposition of a delithiated high energy cathode material, $Li_{1.2-x}Ni_{0.15}Mn_{0.55}Co_{0.1}O_2$, in the stainless-steel high pressure capsules was investigated by in situ high energy X-ray diffraction. The data revealed that the thermally induced decomposition of the delithiated transition metal (TM) oxide was strongly influenced by the presence of electrolyte components. When there was no electrolyte, the layered structure for the delithiated TM oxide was changed to a disordered $Li_{1-x}M_2O_4$-type spinel, which started at ca. 266 °C. The disordered $Li_{1-x}M_2O_4$-type spinel was decomposed to a disordered M_3O_4-type spinel phase, which started at ca. 327 °C. In the presence of organic solvent, the layered structure was decomposed to a disordered M_3O_4-type spinel phase, and the onset temperature of the decomposition was ca. 216 °C. When the $LiPF_6$ salt was also present, the onset temperature of the decomposition was changed to ca. 249 °C with the formation of MnF_2 phase. The results suggest that a proper optimization of the electrolyte component, that is, the organic solvent and the lithium salt, can alter the decomposition pathway of delithiated cathodes, leading to improved safety of lithium-ion batteries.

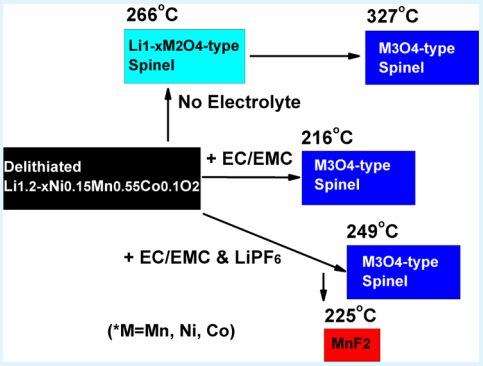

KEYWORDS: *safety, thermal stability, cathode, X-ray diffraction, lithium-ion battery*

INTRODUCTION

Lithium-ion batteries are already used in many kinds of consumer electronic devices, such as cell phones, laptops, and other mobile devices. Worldwide, this energy-storage technology is being evaluated for applications in automobiles, solar farms, wind farms, and electric grids. However, realization of high-energy-density lithium-ion batteries for these applications has been hindered by safety concerns.[1] Several well-publicized safety incidents cast blame on the insufficient safety characteristics of lithium-ion batteries.[2,3]

Although battery manufactures are now able to produce high-quality lithium-ion cells, with less than one reported safety incident for every one million lithium-ion cells produced, the failure rate at the cell level is still too high for transportation or electric grid applications, in which case hundreds or thousands of large-format lithium-ion cells may be packed in series and/or parallel configurations to provide sufficient power and energy output.[4] The failure of a single cell could generate a large amount of heat and trigger thermal runaway of neighboring cells, leading to the propagation of failure throughout the whole battery pack.[5] The overall safety of a battery obviously relates to the thermal stability of each material in the system.[6−8] Therefore, it is important to understand the thermal behavior of lithium-ion battery materials.[9−11]

Cathode materials are stable in the fully lithiated state but exhibit thermal instability when delithiated. The chemical reaction between delithiated cathodes and nonaqueous electrolytes at elevated temperatures (above 200 °C) has long been blamed as the main contributor to the heat generated during the catastrophic failure of lithium-ion batteries. Usually, the thermal stability of delithiated cathodes is characterized by differential scanning calorimetry (DSC),[10,12] accelerating rate calorimetry (ARC),[13−15] or isothermal microcalorimetry (IMC).[16,17] These thermal analysis techniques measure the onset temperature of exothermic reactions and total heat generation profiles. In general, materials with higher onset temperatures or less heat release are considered as possessing better safety. However, detailed information about the nature of these reactions is lacking. Understanding the results from thermal analyses may be further confounded by artifacts

Received: May 2, 2014
Accepted: June 30, 2014
Published: June 30, 2014

introduced during the sample preparation. Rigid controls on the experimental conditions, such as how the sample is prepared, how long it is exposed to the glovebox atmosphere, etc., are required to obtain reproducible results.[13,18] Therefore, systematic understanding of the factors governing the exothermic reactions is still deficient.

Because of the large amounts of gases produced during the exothermic reactions, well-sealed stainless-steel vessels capable of withstanding an internal pressure of hundreds of bars are required to carry out the above thermal analyses. High energy X-ray diffraction (HEXRD) is currently being evaluated as an effective method to probe chemical processes in situ.[19] In this effort, we used HEXRD to investigate the reactions of delithiated $Li_{1.2-x}Ni_{0.15}Mn_{0.55}Co_{0.1}O_2$ with nonaqueous electrolyte sealed in stainless-steel high-pressure capsules and exposed to temperatures up to 400 °C. We chose this active material because the lithium-, manganese-rich, nickel−manganese−cobalt oxide material has been widely studied due to its high specific capacity (>240 mAh/g, when cycled between 2.5 and 4.6 V vs Li^+/Li), low cost, and excellent electrochemical performance at elevated temperatures when compared to other candidate cathode materials.[20]

EXPERIMENTAL SECTION

Materials. The composition of the cathode material used in this study was $Li_{1.2}Ni_{0.15}Mn_{0.55}Co_{0.1}O_2$ with an average particle size of about 4 μm, which was supplied by Toda (HE5050, USA). The cathode laminate consisted of 86 wt % $Li_{1.2}Ni_{0.15}Mn_{0.55}Co_{0.1}O_2$, 8 wt % poly(vinylidene difluoride) (PVDF) binder (Solvay 5130, Belgium), 4 wt % SFG-6 graphite (Timcal, Switzerland), and 2 wt % Super P (Timcal). The thickness of the laminate was about 50 μm, and the loading density was about 6.64 mg of oxide per cm^2.

Samples of delithiated $Li_{1.2-x}Ni_{0.15}Mn_{0.55}Co_{0.1}O_2$ were electrochemically prepared in standard 2032-type coin cells. The cells were assembled in an argon-filled glovebox, and contained a lithium foil as a counter electrode, a microporous polypropylene separator (Celgard 2325), a $Li_{1.2}Ni_{0.15}Mn_{0.55}Co_{0.1}O_2$ electrode, and an appropriate amount of electrolyte. The electrolyte consisted of 1.2 M $LiPF_6$ in a mixture of ethylene carbonate (EC) and ethyl methyl carbonate (EMC) (3:7 by weight). The coin cells were first cycled between 2.5 V and an upper voltage limit of 4.6 V at a C/10 rate (ca. 0.156 mA/cm^2) for two cycles before they were potentiostated at the upper voltage limit. In this paper all potentials are referred to the Li^+/Li potential. After charging, the value of x in the delithiated transition metal (TM) oxide, $Li_{1.2-x}Ni_{0.15}Mn_{0.55}Co_{0.1}O_2$, was estimated from the electrochemical data. We calculated the value of x to be 1.02 (ca. 85% of the active lithium was extracted), assuming that the measured capacity was due to lithium extraction/insertion only.

After delithiation, the cells were disassembled in the glovebox. The harvested electrodes were dipped in dimethyl carbonate (DMC) 40 times in 40 s and dried in the glovebox at room temperature for 1 h. The process is intended to quickly and completely remove the electrolyte residue. As a solid electrolyte interface may exist on the surface of delithiated TM oxide, some compositions of the passivation layer, like organic and inorganic carbonate salts, may be dissolved in DMC. Thus, the dipping process was consistently performed from sample to sample to control the damage of the passivation layer in the same level. Three combinations of the cell materials (designated A, B, and C) were loaded into stainless-steel, high-pressure, differential scanning calorimetry (DSC) capsules (Pyris 1, PerkinElmer, USA). For combination A, 1 mg of the solid material from the harvested electrode was placed in the capsule. For combination B, 1 mg of the solid material was placed in the capsule with 1 μL of electrolyte solvent of EC/EMC in 3:7 ratio by weight. For combination C, 1 mg of the solid material was placed in the capsule with 1 μL of electrolyte consisting of 1.2 M $LiPF_6$ in EC/EMC (3:7 by weight).

In Situ HEXRD. The in situ HEXRD was performed at beamline 11-ID-C of the Advanced Photon Source at Argonne National Laboratory. The experimental setup was similar to that previously reported[19] and is shown in Figure 1. A high energy X-ray beam (115 keV, λ = 0.108 Å) was used because it can penetrate the stainless-steel DSC cell (see Figure 1a). As shown in Figure 1a, a gold-coated copper gasket was used for airtight sealing. The copper gasket will burst through the 1 mm hole in the center of the cap if the internal pressure exceeds 150 bar, which is an overpressure protection. A flower-shaped piece of aluminum was specially designed to keep the solid and liquid samples in the detecting zone even when the polymeric binder melts. The sample was heated to 400 °C at a constant heating rate of 5 °C per minute. The temperature was measured and recorded before and after each XRD exposure. The average of the two point temperatures was used as an indicator of temperature for each XRD pattern.

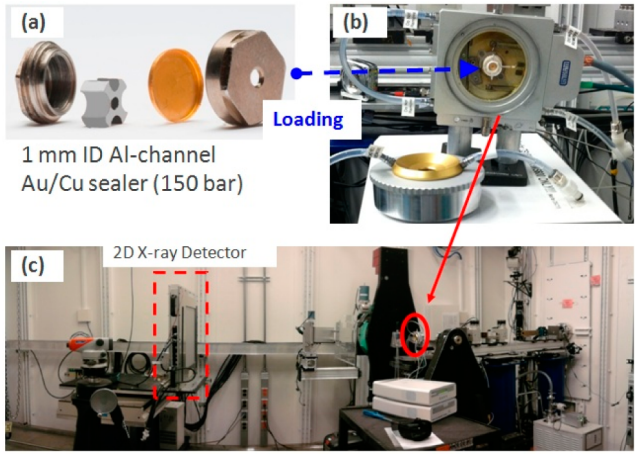

Figure 1. Images of (a) differential scanning calorimetry (DSC) sample holder, (b) programmable furnace, and (c) setup to run in situ HEXRD at Advanced Photon Source of Argonne National Laboratory.

In the course of heating, the transmitted XRD patterns were collected by a PerkinElmer detector at a rate of 1 pattern in 20 s (see Figure 1c). In total, about 225 XRD patterns were taken during the heating with intervals of 1.5 °C. The collected two-dimensional pattern was then integrated into conventional one-dimensional data (intensity vs 2θ) using the fit2d program.[21] For the sake of easy comparison with the results in the literature, all the 2θ values were converted to the values corresponding to Cu Kα_1 radiation (λ = 1.54 Å).

RESULTS AND DISCUSSION

In Situ HEXRD of Combination A. Figure 2 shows a typical HEXRD pattern of the delithiated $Li_{1.2-x}Ni_{0.15}Mn_{0.55}Co_{0.1}O_2$ in the DSC cell at room temperature. The XRD pattern consists of two sets of diffraction patterns: one for the delithiated $Li_{1.2-x}Ni_{0.15}Mn_{0.55}Co_{0.1}O_2$, and the other for the DSC cell. The red dashed line represents the XRD pattern of the empty DSC cell, which was composed of stainless steel, copper, and gold (see Experimental Section).

The 2θ ranges of 34−35, 37.5−39.5, 42−46, 50−52, and 64−65°, where the diffraction peaks of the DSC cell were observed, were excluded in the General Structure Analysis System (GSAS) program,[22,23] and we were able to index delithiated $Li_{1.2-x}Ni_{0.15}Mn_{0.55}Co_{0.1}O_2$ on the basis of the layered $LiMO_2$ structure (M = Ni, Co, and Mn) in the space group $R\bar{3}m$. For the sake of clarity, the diffraction peaks from the DSC cell will be indicated by gray rectangles in the subsequent figures. As will be seen in the following sections, the layered phase was converted to a cubic structure in the space group of $Fd3m$

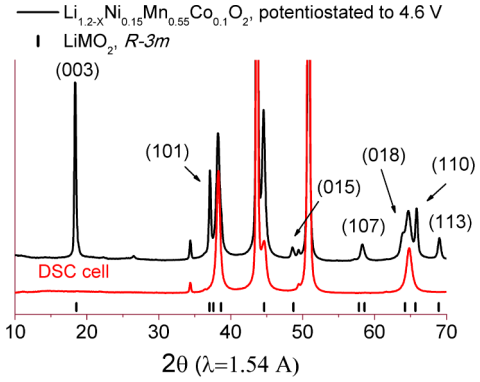

Figure 2. A typical HEXRD pattern of the delithiated $Li_{1.2-x}Ni_{0.15}Mn_{0.55}Co_{0.1}O_2$ in the DSC cell. It shows the characteristic diffraction patterns of DSC cell (red line) and layered $Li_{1.2-x}Ni_{0.15}Mn_{0.55}Co_{0.1}O_2$. For the sake of easy comparison with the results in the literature, all the 2θ values are converted to values corresponding to Cu Kα_1 radiation (λ = 1.54 Å).

(spinel phase). The diffraction peaks originating from the (1) layered phase (2) spinel phase will be subscripted with "L" and "S", respectively.

The HEXRD patterns in Figure 3 show the thermally induced structural changes of the delithiated cathode material during heating. About 55 of these patterns, representing data obtained every 9 °C, are shown in Figure 3a. The delithiated sample had a layered structure at 30 °C. When heated from 30 to 266 °C, the $(003)_L$, $(101)_L$, $(107)_L$, $(018)_L$, $(110)_L$, and $(113)_L$ peaks shifted to smaller 2θ values, showing the thermal expansion of the layered structure. From 266 to 318 °C, the $(018)_L$ peak shifted to a larger 2θ value, gradually closed to the $(110)_L$ peak, and eventually merged with one of the diffraction peaks of the DSC cell at ca. 2θ = 65°. As shown in Figure 3b, the new phase can be indexed to the disordered $Li_{1-x}M_2O_4$-type spinel structure (*Fd*3*m* space group). The positions of the diffraction peaks of the $Li_{1-x}M_2O_4$-type structure are marked by the open square symbol at the bottom of Figures 3−5. The data indicate that the delithiated material changed from a layered structure to a disordered spinel ($Li_{1-x}M_2O_4$ type), which started at ca. 266 °C. The term "disordered spinel" is used here and in the following sections instead of "spinel" to describe the structural type of these phases. Different from the spinel phases that are directly synthesized at high temperature, disordered spinels are usually formed due to cation migration occurring at mild temperatures and are, therefore, not perfectly ordered.[24]

Gradual structural evolution also occurred in the temperature range between 327 and 400 °C. Two diffraction peaks appeared at around 2θ = 30° and 53.5°, and their intensity increased with temperature. As shown in Figure 3b, the new phase can be indexed to the disordered M_3O_4-type spinel structure (*Fd*3*m* space group), and the peaks around 30° and 53.5° represent the $(220)_S$ and $(422)_S$ peaks, respectively. The positions of the diffraction peaks of M_3O_4-type spinel are indicated by the closed square symbols at the bottom of Figures 3−5. The disordered M_3O_4-type phase crystallizes in the same *Fd*3*m* space group as the disordered $Li_{1-x}M_2O_4$-type phase but has larger cell parameters, possessing diffraction peaks at smaller 2θ values, due to the TM cations occupying the tetrahedral sites. The disappearance of the $(333)_S$ and $(531)_S$ peaks and the appearance of $(220)_S$, $(422)_S$, and $(511)_S$ peaks are also consistent with the rearrangement of TM cations in the crystal structure.[25]

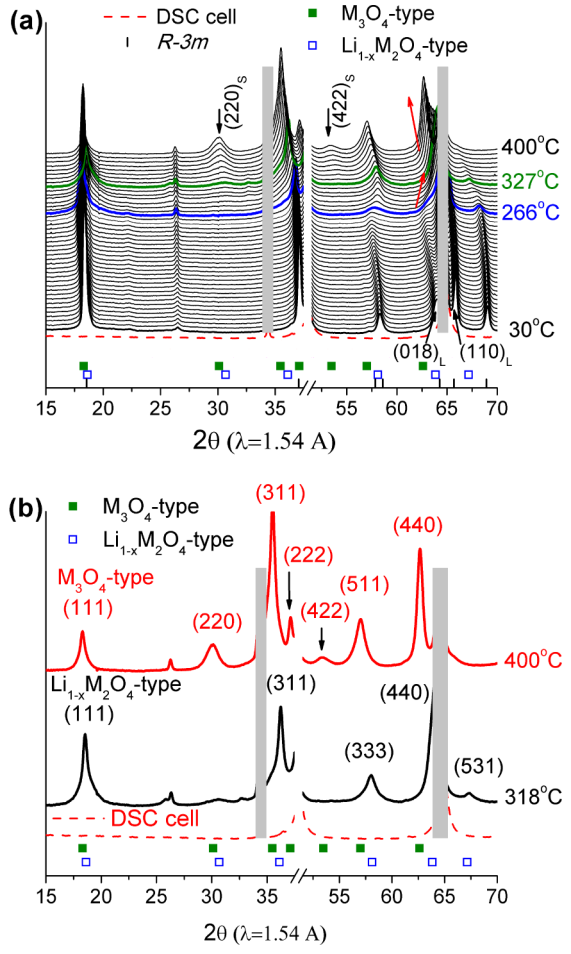

Figure 3. (a) In situ HEXRD patterns of the delithiated $Li_{1.2-x}Ni_{0.15}Mn_{0.55}Co_{0.1}O_2$ (potentiostated to 4.6 V vs Li^+/Li) during heating from room temperature to 400 °C, without the presence of salt or solvent. (b) Two selected XRD patterns from (a) for the sample heated to 318 and 400 °C, showing the fingerprints of disordered $Li_{1-x}M_2O_4$-type and M_3O_4-type spinel phases, respectively. The XRD diffraction peaks from the DSC cell are represented as gray rectangles.

As mentioned by Guilmard et al.,[24] Mn^{2+} can easily move into the tetrahedral site of a close-packed oxygen lattice framework, but moving Mn^{4+} into the tetrahedral site is very difficult. Therefore, the disordered M_3O_4-type spinel phase formation revealed the reduction of the oxidation state of the TM cations. In this case, M_3O_4-type spinel was formed at higher temperature than $Li_{1-x}M_2O_4$-type spinel, being apparently more stable.

In Situ HEXRD of Combination B. To understand the impact of the solvent of electrolyte on the thermal stability of the delithiated cathode, we added EC/EMC (3:7 by weight) to the delithiated TM oxide before heating in the DSC cell. Below 200 °C, no structural changes were observed except thermal expansion of layered structure. Thus, the XRD patterns in this temperature range were not included in Figure 4a. In contrast with the patterns of dry delithiated $Li_{1.2-x}Ni_{0.15}Mn_{0.55}Co_{0.1}O_2$ in Figure 3, Figure 4a shows that phase transformations of the delithiated TM oxide were more complex when heated with solvent.

As shown in Figure 4b, from 201 to 216 °C, the $(107)_L$ and $(018)_L$ peaks barely moved. Above 216 °C, peak shoulders were observed at 2θ = 57 and 62.5° and gradually shifted to smaller 2θ values. This could be assigned to the $(511)_S$ and

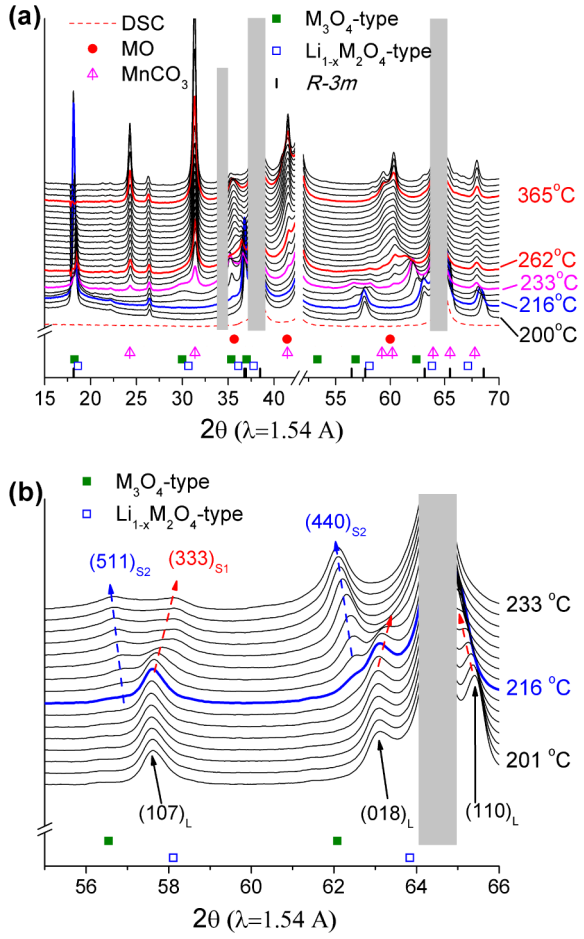

Figure 4. In situ HEXRD patterns of the delithiated $Li_{1.2-x}Ni_{0.15}Mn_{0.55}Co_{0.1}O_2$ (potentiostated to 4.6 V vs Li^+/Li), with the presence of EC/EMC (3:7, by weight), in the temperature range (a) from 200 to 400 °C to show the overall phase transformations and (b) from 200 to 233 °C in a selected 2θ region to show the coexistence of two disordered spinel phases (S1 and S2). The XRD peaks from the DSC cell are represented as gray rectangles.

$(440)_S$ peaks of M_3O_4-type spinel (S2) phase, which was confirmed by the appearance of additional diffraction peak at around 2θ = 30° (Figure 4a). Between 216 and 233 °C, the peaks at 2θ = 57.5 and 63° also shifted toward larger 2θ values. This shows that the $(333)_S$ peak originated from the $(107)_L$, and the $(440)_S$ peak originated from $(018)_L$. The $(018)_L$/$(440)_S$ and $(110)_L$ were gradually overlapped by the diffraction peak of DSC cell at 2θ = 64–65°. Therefore, the merging of $(018)_L$ and $(110)_L$ was obscured, but the peak evolution and position of $(333)_S$ is consistent with the formation of $Li_{1-x}M_2O_4$-type spinel (S1) phase.

Therefore, the data indicate that the onset temperature for phase transformation of delithiated $Li_{1.2-x}Ni_{0.15}Mn_{0.55}Co_{0.1}O_2$ to spinel phases was reduced to 216 °C, in which two disordered spinel phases with two diffraction unit cell parameters simultaneously appeared. This finding indicates that the decomposition of delithiated $Li_{1.2-x}Ni_{0.15}Mn_{0.55}Co_{0.1}O_2$ was facilitated by the presence of the EC/EMC solvent. In addition, it implies that a connection between the formations of two spinel phases was built by the presence of the EC/EMC solvent.

As mentioned above, disordered M_3O_4-type spinel formed with the reduction of TM cations.[24] Here, the solvent facilitated

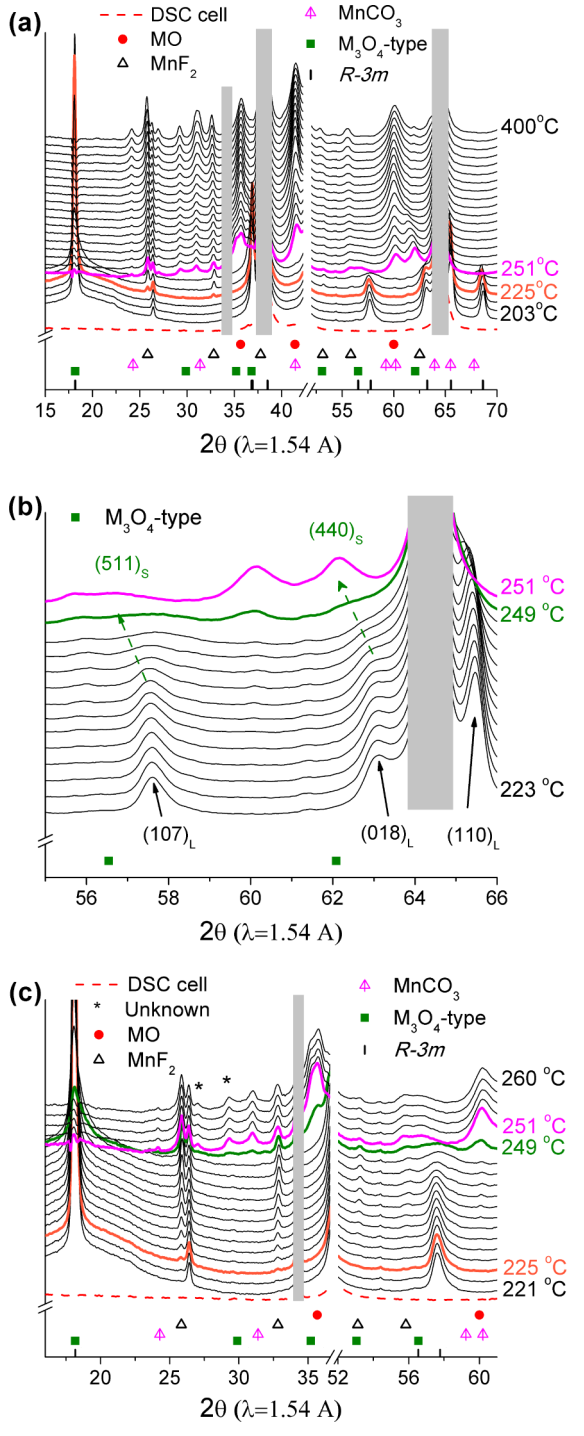

Figure 5. In situ HEXRD patterns of the delithiated $Li_{1.2-x}Ni_{0.15}Mn_{0.55}Co_{0.1}O_2$ (potentiostated to 4.6 V vs Li^+/Li), with the presence of electrolyte, in the temperature range (a) from 203 to 400 °C, (b) from 223 to 251 °C at selected 2θ region of 55–66° to show the phase transformation from $R\bar{3}m$ to disordered M_3O_4-type spinel phases, and (c) from 221 to 260 °C at selected 2θ region of 16–61° to show the onset temperature of MnF_2, MO, and $MnCO_3$ formation. The XRD diffraction peaks from the DSC cell are represented as gray rectangles.

the phase transformation by serving as a reducing agent.[26] Most likely, the accumulation of M_3O_4-type spinel phase in the delithiated TM oxide caused nonreacted layered phase to be

dx.doi.org/10.1021/am502689f | ACS Appl. Mater. Interfaces 2014, 6, 12692–12697

distorted, leading to the movement of the $(018)_L$ and $(110)_L$ peaks above this reduced temperature (216 °C).

Figure 4a also shows that a third phase transformation, mainly represented by the two peaks around 2θ = 24° and 31°, emerged at 233 °C, whose intensity increased with temperature until 400 °C. The appearance of these diffraction peaks are consistent with the formation of $MnCO_3$ (JCPDS No. 44-1472, represented by the umbrella symbol at the bottom of Figures 4a, and 5a,c). The unit cell parameters of the phase were a = 4.782 and c = 15.791 Å at 400 °C. The values were reduced to a = 4.771 and c = 15.646 Å when the sample was cooled to 30 °C, which is consistent with the unit cell parameters of $MnCO_3$ in the JCPDS card (a = 4.773, c = 15.642).

The formation of $MnCO_3$ indicates that the phases present oxidized the EC/EMC solvent, but it is not clear which phase was primarily responsible: the delithiated $Li_{1.2-x}Ni_{0.15}Mn_{0.55}Co_{0.1}O_2$, the disordered M_3O_4-type spinel, or the disordered $Li_{1-x}M_2O_4$-type spinel.

The fourth phase transformation, as shown in Figure 4a, is indicated by the evolution of a set of peaks around 2θ = 36°, 41°, and 60° between 262 and 400 °C. Above 262 °C, the peak at 2θ = 36° and the shoulders of peaks at 2θ = 41 and 60° were observed. The diffraction peak and shoulders can be indexed as an MO-type rock-salt phase ($Fm3m$), where M is a mixture of Ni, Co, and Mn. Above 365 °C, the peak at 2θ = 36° and the shoulders of peaks at 2θ = 41° were gradually vanished, and the broad peak at 2θ = 60° seemed to split. The data indicate that the MO-type rock-salt phase formed above 262 °C but started to vanish at ca. 365 °C. Instead, above 365 °C, additional $MnCO_3$ appeared.

In Situ HEXRD of Combination C. To understand the effect of the electrolyte on the thermal stability, $LiPF_6$ with EC/EMC (3:7 by weight) was added to the delithiated TM oxide before heating in the DSC cell. The phase transformations (see Figure 5a) started at 225 °C, and many changes in the XRD patterns were observed within the next 30 °C. Figure 5b shows an enlarged view of the patterns obtained in the temperature range of 223 to 251 °C for the 2θ range of 55−66°. From 223 to 242 °C, the position of $(017)_L$, $(018)_L$, and $(110)_L$ peaks barely moved. Above 249 °C, the $(107)_L$ and $(018)_L$ peaks gradually shifted to smaller 2θ values and smeared, which was followed by the appearance of $(511)_S$ and $(440)_S$ peaks at 251 °C. The evolution of peaks at 58 and 62° (also 30 and 35°, see Figure 5a) suggest the formation of disordered M_3O_4-type spinel originating from layered structure. The onset temperature of the layered-to-spinel phase transformation increased by ca. 30 °C in comparison with that shown in Figure 4b (no $LiPF_6$ present). In other words, the thermal stability of delithiated TM oxide in organic solvent was increased.

Furthermore, emerging diffraction peaks, mainly at 26 and 33°, were observed above 225 °C (Figure 5a,c) and did not disappear with further heating to 400 °C. These diffraction peaks can be indexed to MnF_2 (JCPDS No. 24−0727). The unit cell parameters of this phase were a = 4.885 Å and c = 3.299 Å when the sample was cooled to 30 °C, which is consistent with the unit cell parameters of MnF_2 in the JCPDS card (a = 4.8736 Å, c = 3.31 Å).

The MnF_2 phase may play an important role since the transformation temperature of the layered phase to disordered M_3O_4-type spinel increased by ca. 30 °C. As reported by Chen et al.,[19] the MnF_2 phase may arise from the decomposition of $LiPF_6$. The decomposed $LiPF_6$, such as PF_5, is a strong Lewis acid, which can etch the delithiated TM oxide to yield MnF_2.[19,27]

PROPOSED MECHANISM

We summarize the above observations in Scheme 1, which illustrates how the carbonate solvent (EC/EMC) and lithium salt ($LiPF_6$) influence the early decomposition of the delithiated $Li_{1.2-x}Ni_{0.15}Mn_{0.55}Co_{0.1}O_2$. The decomposition of delithiated $Li_{1.2-x}Ni_{0.15}Mn_{0.55}Co_{0.1}O_2$ goes through the disordered M_3O_4-type spinel phase, where the valence state of the TM cations is reduced. Without the presence of other media, the reduction can only be achieved through oxygen evolution from the structural lattice, as it was reported for other delithiated TM oxide.[28] The presence of solvent provides an electron-rich environment. Then, the valence state of TM cations is reduced through the electron transfer from the oxidation of the solvent to the delithiated $Li_{1.2-x}Ni_{0.15}Mn_{0.55}Co_{0.1}O_2$. The process is evidenced by the formation of a large amount of oxidation product, $MnCO_3$ phase, and the reduced onset temperature for the formation of disordered M_3O_4-type spinel phase. When the electron transfer is interfered by the less conductive materials, such as MnF_2 phase, the oxidation of solvent and decomposition of delithiated $Li_{1.2-x}Ni_{0.15}Mn_{0.55}Co_{0.1}O_2$ are slowed down. Then, the thermal stability of delithiated $Li_{1.2-x}Ni_{0.15}Mn_{0.55}Co_{0.1}O_2$ in organic solvent is increased.

Scheme 1. Phase Transformations of the Delithiated $Li_{1.2-x}Ni_{0.15}Mn_{0.55}Co_{0.1}O_2$ (Potentiostated to 4.6 V vs Li^+/Li) during Heating[a]

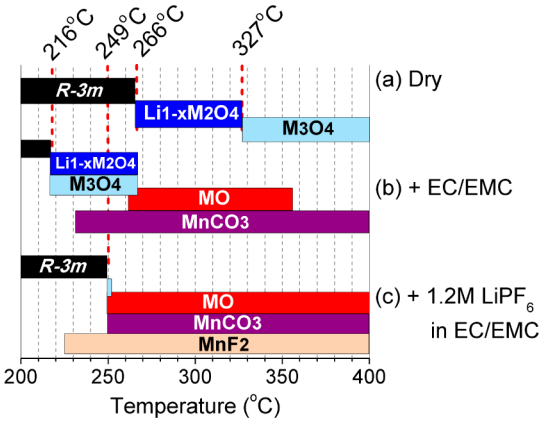

[a](a) Without solvent or lithium salt. (b) With EC/EMC solvent (3:7, weight). (c) With electrolyte of 1.2 M $LiPF_6$ in EC/EMC (3:7, by weight). On the basis of the *in-situ* HEXRD data in Figures 3−5.

CONCLUSIONS

The thermally induced decomposition of delithiated TM oxide is sensitive to the chemical environment since it is related to the reduction of TM cations. A dry sample (no electrolyte) of this material decomposes above 327 °C. The organic electrolyte solvent (EC/EMC) acts as an electron source to facilitate the reduction of TM cations. The formation of manganese fluoride (MnF_2) with the presence of $LiPF_6$ reduces the active surface area for electron transfer between the delithiated TM oxide and the solvent and, therefore, increases the thermal stability of delithiated TM oxide in the presence of solvent.

AUTHOR INFORMATION

Corresponding Author

*E-mail: zonghai.chen@anl.gov. Phone: 630-252-6551.

Notes

The authors declare no competing financial interest.

ACKNOWLEDGMENTS

Research at Argonne National Laboratory was funded by U.S. Department of Energy (DOE), Office of Vehicle Technologies. Argonne National Laboratory is operated for the U.S. DOE by UChicago Argonne, LLC, under Contract No. DE-AC02-06CH11357. The authors also acknowledge the use of the Advanced Photon Source of Argonne National Laboratory supported by the U.S. DOE, Office of Science, Office of Basic Energy Sciences. The cathodes were produced at the U.S. DOE Cell Analysis, Modeling and Prototyping (CAMP) facility, Argonne National Laboratory. The CAMP facility at Argonne is fully supported by the DOE Vehicle Technologies Program (VTP) within the core funding of the Applied Battery Research (ABR) for Transportation Program.

REFERENCES

(1) Tsujikawa, T.; Yabuta, K.; Arakawa, M.; Hayashi, K. Safety of Large-Capacity Lithium-ion Battery and Evaluation of Battery System for Telecommunications. *J. Power Sources* **2013**, *244*, 11−16.

(2) Ostrower, J.; Pasztor, A. *Microscopic "Dendrites" a Focus in Boeing Dreamliner Probe;* The Wall Street Journal: New York, NY, 2013. http://online.wsj.com/news/articles/SB10001424127887324880504578298673566960476 (accessed Feb 11, 2013).

(3) Lees, A. B. Ensuring Boeing's Lithium-Ion Battery Safety. *Chem. Eng. News* **2013**, *91*, 4−4.

(4) Choi, N.-S.; Chen, Z.; Freunberger, S. A.; Ji, X.; Sun, Y.-K.; Amine, K.; Yushin, G.; Nazar, L. F.; Cho, J.; Bruce, P. G. Challenges Facing Lithium Batteries and Electrical Double-Layer Capacitors. *Angew. Chem., Int. Ed.* **2012**, *51*, 9994−10024.

(5) Wang, Q.; Ping, P.; Zhao, X.; Chu, G.; Sun, J.; Chen, C. Thermal Runaway Caused Fire and Explosion of Lithium Ion Battery. *J. Power Sources* **2012**, *208*, 210−224.

(6) Idota, Y.; Kubota, T.; Matsufuji, A.; Maekawa, Y.; Miyasaka, T. Tin-Based Amorphous Oxide: A High-Capacity Lithium-Ion-Storage Material. *Science* **1997**, *276*, 1395−1397.

(7) Chen, Z.; Ren, Y.; Jansen, A. N.; Lin, C.-k.; Weng, W.; Amine, K. New Class of Nonaqueous Electrolytes for Long-Life and Safe Lithium-Ion Batteries. *Nat. Commun.* **2013**, *4*, 1513.

(8) He, Y.-B.; Ling, G.-W.; Tang, Z.-Y.; Song, Q.-S.; Yang, Q.-H.; Chen, W.; Lv, W.; Su, Y.-J.; Xu, Q. Safety Properties of Liquid State Soft Pack High Power Batteries with Carbon-Coated LiFePO4/Graphite Electrodes. *J. Solid State Electrochem.* **2010**, *14*, 751−756.

(9) Yabuuchi, N.; Ohzuku, T. Novel Lithium Insertion Material of LiCo1/3Ni1/3Mn1/3O2 for Advanced Lithium-Ion Batteries. *J. Power Sources* **2003**, *119*, 171−174.

(10) Belharouak, I.; Lu, W.; Liu, J.; Vissers, D.; Amine, K. Thermal Behavior of Delithiated Li(Ni0.8Co0.15Al0.05)O2 and Li1.1(Ni1/3Co1/3Mn1/3)0.9O2 Powders. *J. Power Sources* **2007**, *174*, 905−909.

(11) Gao, Y. A.; Yakovleva, M. V.; Ebner, W. B. Novel LiNi1-xTix/2Mgx/2O2 Compounds as Cathode Materials for Safer Lithium-Ion Batteries. *Electrochem. Solid-State Lett.* **1998**, *1*, 117−119.

(12) Bang, H.; Kim, D.-H.; Bae, Y. C.; Prakash, J.; Sun, Y.-K. Effects of Metal Ions on the Structural and Thermal Stabilities of Li [Ni1 − x − yCoxMny] O2 ($x + y \leq 0.5$) Studied by In Situ High Temperature XRD. *J. Electrochem. Soc.* **2008**, *155*, A952−A958.

(13) MacNeil, D. D.; Dahn, J. R. Test of Reaction Kinetics Using Both Differential Scanning and Accelerating Rate Calorimetries As Applied to the Reaction of LixCoO2 in Non-aqueous Electrolyte. *J. Phys. Chem. A* **2001**, *105*, 4430−4439.

(14) Luo, W.; Zhou, F.; Zhao, X.; Lu, Z.; Li, X.; Dahn, J. R. Synthesis, Characterization, and Thermal Stability of LiNi1/3Mn1/3Co1/3−zMgzO2, LiNi1/3−zMn1/3Co1/3MgzO2, and LiNi1/3Mn1/3−zCo1/3MgzO2. *Chem. Mater.* **2010**, *22*, 1164−1172.

(15) Luo, W. B.; Li, X. H.; Dahn, J. R. Synthesis, Characterization, and Thermal Stability of Li[Ni1/3Mn1/3Co1/3-z(MnMg)(z/2)]O2. *Chem. Mater.* **2010**, *22*, 5065−5073.

(16) Lu, W.; Belharouak, I.; Park, S. H.; Sun, Y. K.; Amine, K. Isothermal Calorimetry Investigation of Li1+x Mn2−y Al z O4 Spinel. *Electrochim. Acta* **2007**, *52*, 5837−5842.

(17) Lu, W.; Belharouak, I.; Liu, J.; Amine, K. Thermal Properties of Li4/3Ti5/3O4/LiMn2O4 Cell. *J. Power Sources* **2007**, *174*, 673−677.

(18) Barnett, B. M. In *New Directions in Battery Safety: Prospects for Fail Safe Lithium-Ion;* Battery Safety 2010 Conference, Boston, MA, Nov 3, 2010; TIAX LLC Lexington, MA, 2010.

(19) Chen, Z.; Ren, Y.; Lee, E.; Johnson, C.; Qin, Y.; Amine, K. Study of Thermal Decomposition of Li1-x(Ni1/3Mn1/3Co1/3)0.9O2 Using In-Situ High-Energy X-Ray Diffraction. *Adv. Energy Mater.* **2013**, *3*, 729−736.

(20) Kim, D.; Croy, J. R.; Thackeray, M. M. Comments on Stabilizing Layered Manganese Oxide Electrodes for Li Batteries. *Electrochem. Commun.* **2013**, *36*, 103−106.

(21) Hammersley, A. P.; Svensson, S. O.; Hanfland, M.; Fitch, A. N.; Hausermann, D. Two-Dimensional Detector Software: From Real Detector to Idealised Image or Two-Theta Scan. *High Pressure Res.* **1996**, *14*, 235−248.

(22) Larson, A. C.; Dreele, R. B. V. *General Structure Analysis System (GSAS);* Technical Report LAUR 86−748 for the Los Alamos National Laboratory, Los Alamos, NM, 2004.

(23) Toby, B. EXPGUI, a Graphical User Interface for GSAS. *J. Appl. Crystallogr.* **2001**, *34*, 210−213.

(24) Guilmard, M.; Croguennec, L.; Denux, D.; Delmas, C. Thermal Stability of Lithium Nickel Oxide Derivatives. Part I: LixNi1.02O2 and LixNi0.89Al0.16O2 (x = 0.50 and 0.30). *Chem. Mater.* **2003**, *15*, 4476−4483.

(25) Nam, K.-W.; Yoon, W.-S.; Yang, X.-Q. Structural Changes and Thermal Stability of Charged LiNi1/3Co1/3Mn1/3O2 Cathode Material for Li-Ion Batteries Studied by Time-Resolved XRD. *J. Power Sources* **2009**, *189*, 515−518.

(26) Yamamoto, K.; Minato, T.; Mori, S.; Takamatsu, D.; Orikasa, Y.; Tanida, H.; Nakanishi, K.; Murayama, H.; Masese, T.; Mori, T.; Arai, H.; Koyama, Y.; Ogumi, Z.; Uchimoto, Y. Improved Cyclic Performance of Lithium-Ion Batteries: An Investigation of Cathode/Electrolyte Interface via In Situ Total-Reflection Fluorescence X-ray Absorption Spectroscopy. *J. Phys. Chem. C* **2014**, *118*, 9538−9543.

(27) Myung, S. T.; Amine, K.; Sun, Y. K. Surface Modification of Cathode Materials from Nano- to Microscale for Rechargeable Lithium-Ion Batteries. *J. Mater. Chem.* **2010**, *20*, 7074−7095.

(28) Bak, S. M.; Nam, K. W.; Chang, W.; Yu, X. Q.; Hu, E. Y.; Hwang, S.; Stach, E. A.; Kim, K. B.; Chung, K. Y.; Yang, X. Q. Correlating Structural Changes and Gas Evolution during the Thermal Decomposition of Charged LixNi0.8Co0.15Al0.05O2 Cathode Materials. *Chem. Mater.* **2013**, *25*, 337−351.